

Regularizing Parameterized Kerr Spacetime

Samantha Lomuscio

Fair Lawn, New Jersey, USA

B.S. Applied Physics, New Jersey Institute of Technology, 2020

A Thesis presented to the Graduate Faculty
of the University of Virginia in candidacy for the Degree of
Master of Science

Department of Physics

University of Virginia

May 2023

Committee

Professor Kent Yagi, *Research Advisor*

Professor David Nichols

Abstract

Deviations from General Relativity (GR) may become large and detectable in extreme environments with strong and dynamic gravitational fields, such as those around rotating black holes. Various parameterized Kerr spacetimes have been proposed to perform strong-field tests with black hole observations in a theory-agnostic way. Some of these parameterized Kerr spacetimes are constructed such that the modified black hole spacetimes still possess certain symmetries of the Kerr black hole. Such symmetry-preserving spacetimes consist of arbitrary functions of the radial coordinate that capture deviations from Kerr in GR. Practically, one expands these functions about infinity and truncates to extract a finite number of deviation parameters. We find this truncation can introduce pathologies such as nonphysical divergences. To overcome this, we take two different attempts: (i) rescale the arbitrary functions, and (ii) treat the non-GR deviations as small perturbations in the parameterized Kerr spacetime, expand, and keep to linear order in the deviation. We then map black hole solutions in several example non-GR theories to the refined parameterized metric and quantify how well the latter can recover the former with a root-mean-square error

analysis. We find that both the rescaling and small deviation approximation attempts can remedy the fictitious divergences seen with the original expansion in most cases. Additionally, we find overall the parameterized metric does fairly well at recovering the existing beyond-GR metrics in many cases and can even recover some non-GR solutions exactly.

Acknowledgments

I would like to extend my most sincere thanks to my advisor, Kent Yagi, for teaching me everything I know about gravity and for being an excellent example of what a great researcher is. I really appreciate him answering my every question in our many meetings and for reviewing my every calculation. I truly value all the time he has put in to be a great mentor and friend to me. His unwavering support and guidance were instrumental in my completion of this thesis and my growth as a person.

I also would like to thank David Nichols for being a member of my thesis committee. I truly appreciate the time he took from his schedule to review this work and attend my defense.

Additionally, I want to thank my classmates and good friends including Sid Ajith, Annika Siddarth, Birch Ely, Gabriel Sousa, Sarah Nicholson, Anchit Arora, and Chris Martin, whose enlightening discussions greatly strengthened my love for and understanding of physics, and whose friendship I will always cherish.

Lastly, I want to thank my parents, Barbara and Ronald Lomuscio, and my sister, Melissa Lomuscio, for their constant support of my every pursuit and for always

listening to me talk about black holes and our universe for hours on end. They have shaped me into the person I am today and have instilled in me my love for learning. Their encouragement and love has given me the confidence and motivation to tackle this project, and without which I would not be where I am today.

List of Figures

1.1	Nonphysical divergence in original CY metric	16
2.1	Rescaled CY Metric for Braneworld Example	23
2.2	Rescaled CY Metric for EdGB Example	27
2.3	Kerr-Sen Rescaled Sixth Order Expansion $t\phi$ Divergence	28
3.1	tt component of CY Mapped to Braneworld with Approach 1 Parameterization	37
3.2	Nonphysical Divergence in $t\phi$ component of CY mapped to dCS with expanded Approach 1	39
3.3	tt component of CY Mapped to Braneworld with Approach 2 Parameterization	41
3.4	tt component of CY Mapped to Braneworld with Approach 3 Parameterization	44
C.1	Kerr-Sen tt Component Double Expansion	70

List of Tables

2.1	RMSE Values for Rescaled \mathcal{A}_i	25
3.1	RMSE Values for Approach 1 of Small Deviation Approximation . . .	33
3.2	RMSE Values for Approach 2 of Small Deviation Approximation . . .	34
3.3	RMSE Values for Approach 3 of Small Deviation Approximation . . .	35
B.1	RMSE with Varied θ and a	66

Contents

Abstract	1
Acknowledgments	3
1 Introduction	9
1.1 Background	9
1.2 CY Parameterized Black Hole Metric	12
2 Rescaling \mathcal{A}_i Mappings	18
2.1 Rescaling	18
2.2 Results and Discussion	21
3 Small Deviation Approximation	29
3.1 Finding $\delta\mathcal{A}_i$ Mappings	30
3.2 Results and Discussion	31
3.2.1 Approach 1: $n = -1$	36
3.2.2 Approach 2: $n = 0$	38

<i>CONTENTS</i>	8
3.2.3 Approach 3: $n = 1$	42
3.3 Summary	43
4 Conclusion	46
A Example Theories	54
A.1 Braneworld	54
A.2 Kerr-Sen	56
A.3 EdGB	57
A.4 dCS	59
A.5 Bardeen	60
A.6 Kalb-Ramond	61
B RMSE with varied θ and a	64
C Konoplya-Rezzolla-Zhidenko Metric	67

Chapter 1

Introduction

1.1 Background

For hundreds of years, Isaac Newton's law of universal gravitation was widely accepted as *the* theory of gravity. Although Newton's theory very successfully described forces of attraction between masses, it failed to give explanations for several astronomical observations. For example, Newtonian gravity could not correctly explain the rate of precession of Mercury's perihelion, nor could it explain the apparent deflection of starlight around the Sun. These shortcomings in Newton's formulation of gravity stumped the scientific community until 1915, about 300 years after Newton, with Albert Einstein's development of the Theory of General Relativity (GR).

Einstein's pursuit of a new theory of gravity and his drive to reconcile these inconsistencies in the existing classical physics is what led him to construct the famous

GR, which revolutionized our understanding of the nature of our universe and has had a profound impact on modern physics and cosmology. In a nutshell, this complex theory elegantly describes gravity as a geometric phenomenon – it is the curvature of spacetime caused by the presence of matter stress-energy.

To everyone’s excitement, this new theory did in fact reconcile many existing issues in physics, particularly those issues with Newton’s theory of gravity. GR correctly predicted the precession of Mercury’s orbit and predicted the phenomenon of gravitational lensing, thus explaining how and why starlight is deflected around the Sun. It also predicted novel phenomena including gravitational waves – ripples, or perturbations, in the fabric of spacetime caused by the acceleration of massive objects.

Today, GR has been extensively tested, and has passed every test with flying colors [1]. GR has been studied with e.g. solar system experiments [1, 2] and binary pulsar observations [3, 4] that probe gravity in the weak, non-dynamical field regime.

Despite GR’s unprecedented success, we continue to study gravity because a few issues still remain. GR is incompatible with quantum mechanics and we have been unable to unite gravity with the three other fundamental forces: the strong interaction, the weak interaction, and electromagnetism. This mismatch in fundamental theories indicates that something is missing. Additionally, we do not understand the nature of dark energy and dark matter that drive the expansion of the universe and the rotation of galaxies, respectively, and we do not have an explanation for the extreme matter/anti-matter asymmetry that is present in our universe. A new theory of

gravity that extends beyond GR can provide answers to these fundamental questions [5, 6, 7]. Here we find ourselves in a similar position as Einstein found himself in the early 1900s; unexplained phenomena still drive our pursuit to better understand and more accurately describe the nature of gravity and our universe.

As mentioned above, GR's success has been confirmed by experiments that tested the theory in the weak, non-dynamical field regime – no deviations from GR have been found where gravity is weak. If deviations from GR do in fact exist, we expect that more extreme environments, where the gravitational field is strong and dynamic, will make the deviations more evident and easier to detect. This is because in regions of intense gravity signatures of even small deviations can be amplified and then detected. The spacetime surrounding black holes fits this description perfectly and is therefore a natural choice for where we should look for these deviations from GR.

An important consequence of GR is the no-hair theorem. This theorem states that isolated, stationary, uncharged black holes are uniquely characterized by the Kerr metric, which completely describes these objects with only two parameters, their mass M and their spin, a , where $a \equiv J/M$, and J is the angular momentum [8, 9]. In other words, astrophysical black holes only have two “hairs” and are always described by the Kerr metric. This metric is a vacuum solution to the Einstein field equations and is stationary, axisymmetric, asymptotically flat, and contains an event horizon that enshrouds a central singularity. Properties of black holes and the no-hair theorem have been tested through black hole shadows [10, 11], orbits of supermassive

black hole (SMBH) stellar companions [12, 13, 14], and quasinormal ringdown modes of post-merger colliding black holes [15, 16, 17] to name a few.

There are many beyond-GR theories of gravity whose theoretical spacetimes contain deviations from Kerr and describe black holes with more “hairs” than just mass and spin. The black holes in these theories are thus not described by the Kerr metric. Studying the spacetime around black holes can allow us to determine if these extra hairs are present.

An efficient way to test gravity for these potential non-Kerr effects is to construct a beyond-Kerr spacetime metric in a generic, theory-agnostic way. This spacetime should deviate from Kerr parametrically and recover Kerr when the deviations themselves vanish. Spacetimes like this have been constructed: e.g.) Johannsen [18], Konoplya [19], and Carson and Yagi [20]. We can take a generic parameterized metric and map it to specific beyond-GR theories to determine if the metric can recover existing theories of gravity.

1.2 CY Parameterized Black Hole Metric

Let us look at the Carson and Yagi (CY) metric in detail. This metric maintains Kerr-symmetries: it is stationary, axisymmetric, asymptotically flat, and has a separable structure [20]. The metric provides separable geodesic equations that lead to no chaotic orbits, and has four constants of motion, proper mass, energy, angular momentum, and Carter constant. The CY metric is a generalization of the Johannsen

metric and the former includes an additional arbitrary function. The CY metric is given by¹

$$g_{tt} = -\frac{\tilde{\Sigma} (\Delta - a^2 \mathcal{A}_2 \sin^2 \theta)}{\tilde{\rho}^4}, \quad (1.2)$$

$$g_{rr} = \frac{\tilde{\Sigma}}{\mathcal{A}_5 \Delta}, \quad (1.3)$$

$$g_{\theta\theta} = \tilde{\Sigma}, \quad (1.4)$$

$$g_{\phi\phi} = \frac{\tilde{\Sigma} \sin^2 \theta \left[(a^2 + r^2)^2 \mathcal{A}_1 - a^2 \Delta \sin^2 \theta \right]}{\tilde{\rho}^4}, \quad (1.5)$$

$$g_{t\phi} = -\frac{a \tilde{\Sigma} \sin^2 \theta \left[(a^2 + r^2) \mathcal{A}_0 - \Delta \right]}{\tilde{\rho}^4}, \quad (1.6)$$

where

$$\begin{aligned} \tilde{\rho}^4 &= a^4 \mathcal{A}_2 \sin^4 \theta + (a^2 + r^2)^2 \mathcal{A}_1 \\ &\quad + a^2 (a^2 + r^2) \left(\frac{a^2 + r^2}{\Delta} (\mathcal{A}_0^2 - \mathcal{A}_1 \mathcal{A}_2) - 2\mathcal{A}_0 \right) \sin^2 \theta, \end{aligned} \quad (1.7)$$

and

$$\tilde{\Sigma} \equiv \Sigma + f(r) + g(\theta), \quad (1.8)$$

$$\Sigma = r^2 + a^2 \cos^2 \theta, \quad (1.9)$$

$$\Delta = r^2 - 2Mr + a^2. \quad (1.10)$$

¹The original CY metric used the radial functions $A_i(r)$ while we introduced $\mathcal{A}_i(r)$. These two sets are related by

$$(\mathcal{A}_0, \mathcal{A}_1, \mathcal{A}_2, \mathcal{A}_5) = (A_0, A_1^2, A_2^2, A_5). \quad (1.1)$$

This is because A_1 and A_2 only enter in the metric through A_1^2 and A_2^2 .

Here M and a are the mass and Kerr spin parameter of the black hole, $\mathcal{A}_i(r)$ are arbitrary functions of r , $f(r)$ and $g(\theta)$ are arbitrary functions of r and θ , respectively. We can set $g(\theta) = 0$ to satisfy solar system bounds. The above metric reduces to the Kerr black hole when $\mathcal{A}_i \rightarrow 1$ and $f(r) \rightarrow 0$, while it reduces to the Johannsen metric [18] in the limit $\mathcal{A}_0^2 \rightarrow \mathcal{A}_1\mathcal{A}_2$.

The CY metric [20] exhibits pathologies in certain situations. The metric itself consists of five functions of the radial coordinate, r , that capture the deviations from Kerr. When mapping this metric to existing beyond-GR theories, these functions are expanded about $r = \infty$. The expansion coefficients represent the deviation parameters from Kerr. Naturally, these are infinite expansions, so for practical purposes we truncate the expansion, so as to have a finite number of beyond-Kerr deviation parameters. This truncation can introduce pathological behavior, such as nonphysical divergences, into the spacetime.

As an example, let us look at the tt component of the Braneworld black hole [21] in the Randall-Sundrum model [22, 23] compared to the tt component of the CY metric [20] mapped to Braneworld to highlight this pathological behavior, see Figure 1.1. The Braneworld metric has the following form:

$$\begin{aligned}
 ds^2 = & - \left(1 - \frac{2Mr - \beta}{\Sigma} \right) dt^2 - \frac{2a(2Mr - \beta)}{\Sigma} \sin^2 \theta dt d\phi \\
 & + \frac{\Sigma}{\beta + \Delta} dr^2 + \Sigma d\theta^2 + \left(r^2 + a^2 + \frac{2Mr - \beta}{\Sigma} a^2 \sin^2 \theta \right) \sin^2 \theta d\phi^2.
 \end{aligned} \tag{1.11}$$

Here, β is the beyond-Kerr parameter for this theory. Specifically, it is a tidal charge parameter originating from some nonlocal gravitational effects due to a five-

dimensional bulk spacetime.

One can see in Figure 1.1 the gravitational potential as a function of the radial coordinate r . Here we show this potential ranging from the event horizon to twice the event horizon and normalize it to the black hole mass. The true potential is shown by the solid blue curve and the spacetime from [20] mapped to Braneworld with a truncated series is shown by the red dashed line. In the truncated parameterized spacetime, we see a nonphysical divergence near the event horizon. This artificial divergence will pose a problem when comparing the parameterized spacetime with spacetimes from black hole observations; there will be a mismatch as there is a divergence in the model where there should not be any such divergence in real life.

The goal of this work is to refine the CY metric presented in [20] in such a way that it no longer exhibits pathological behavior like this nonphysical divergence. In our attempts to remedy the fictitious divergence, we changed the form of the arbitrary functions of r in the CY metric in different ways. In the first attempt, we rescaled the arbitrary functions of r in the CY metric by one of the arbitrary functions themselves and by a factor of Δ . In the second attempt, we treated the deviations from Kerr as small perturbations and parameterized the arbitrary functions of r by Δ^n with $n = -1, 0, 1$. We will describe these in-depth in Chapter 3.

Let us now go through the process of finding the rescaled mapping functions between CY and a selected existing beyond-GR metric, which we will refer to as

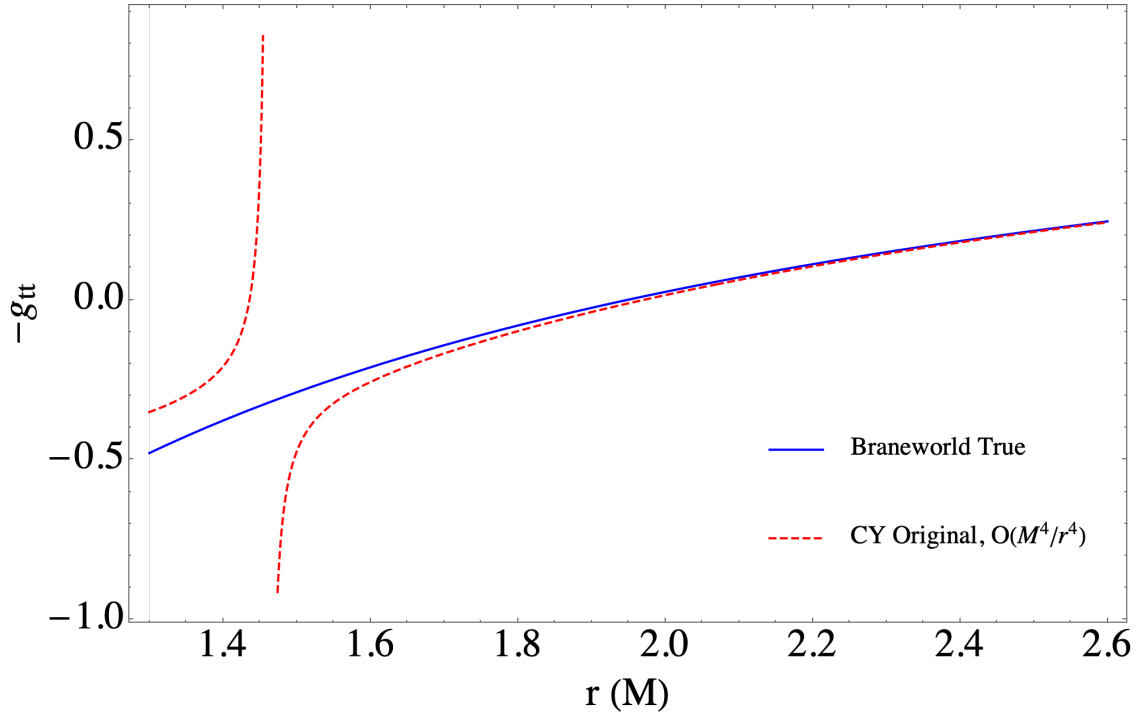


Figure 1.1: Nonphysical divergence exhibited by the CY metric for the Braneworld example. We plot the tt component of the metric for the true Braneworld black hole (blue solid) and the original CY metric with the mapping functions \mathcal{A}_i expanded about $r = \infty$ (red dashed). We choose parameter values $\theta = \frac{\pi}{2}$, $a = 0.9$, $M = 1$, and $\beta = 0.1$.

X . First, equate the refined CY metric components (detailed in Section 1.2) with the corresponding components of metric X to find a system of equations that we can solve for $\mathcal{A}_0(r)$, $\mathcal{A}_1(r)$, $\mathcal{A}_2(r)$, $\mathcal{A}_5(r)$, and $f(r)$ as a function of the beyond-Kerr parameters present in metric X . These are what we will call the mapping functions.

Chapter 2

Rescaling \mathcal{A}_i Mappings

In this attempt to remove the nonphysical divergence, we rescale the $\mathcal{A}_i(r)$ functions by $\mathcal{A}_5(r)$ and factor out Δ . We make no assumptions about the size of the deviation from Kerr – in this attempt we do not assume the deviation to be small as we do in Chapter 3.

2.1 Rescaling

We rescale \mathcal{A}_5 first by factoring out Δ , and call this $\bar{\mathcal{A}}_5$. We then rescale \mathcal{A}_0 , \mathcal{A}_1 , and \mathcal{A}_2 by $\bar{\mathcal{A}}_5$ and a factor of Δ . We will follow the notation $\bar{\mathcal{A}}_i$ to denote rescaled functions.

$$\mathcal{A}_5 \rightarrow \frac{\bar{\mathcal{A}}_5}{\Delta}, \quad (2.1)$$

$$\mathcal{A}_0 \rightarrow \frac{\bar{\mathcal{A}}_0 \Delta}{\bar{\mathcal{A}}_5}, \quad (2.2)$$

$$\mathcal{A}_1 \rightarrow \frac{\bar{\mathcal{A}}_1 \Delta}{\bar{\mathcal{A}}_5}, \quad (2.3)$$

$$\mathcal{A}_2 \rightarrow \frac{\bar{\mathcal{A}}_2 \Delta}{\bar{\mathcal{A}}_5}. \quad (2.4)$$

The CY metric with these rescaled functions becomes

$$g_{tt} = \frac{\tilde{\Sigma} \bar{\mathcal{A}}_5 \csc^2 \theta (\bar{\mathcal{A}}_5 \csc^2 \theta - a^2 \bar{\mathcal{A}}_2)}{\bar{\rho}}, \quad (2.5)$$

$$g_{rr} = \frac{\tilde{\Sigma}}{\bar{\mathcal{A}}_5}, \quad (2.6)$$

$$g_{\theta\theta} = \tilde{\Sigma}, \quad (2.7)$$

$$g_{\phi\phi} = \frac{\tilde{\Sigma} \bar{\mathcal{A}}_5 \sin^2 \theta [\bar{\mathcal{A}}_1 (a^2 + r^2)^2 - a^2 \bar{\mathcal{A}}_5 \sin^2 \theta]}{\bar{\rho}}, \quad (2.8)$$

$$g_{t\phi} = \frac{a \tilde{\Sigma} \bar{\mathcal{A}}_5 \csc^2 \theta [(a^2 + r^2) \bar{\mathcal{A}}_0 - \bar{\mathcal{A}}_5]}{\bar{\rho}}, \quad (2.9)$$

where

$$\begin{aligned} \bar{\rho} = & a^4 \bar{\mathcal{A}}_2 \bar{\mathcal{A}}_5 + \bar{\mathcal{A}}_1 \bar{\mathcal{A}}_5 (a^2 + r^2)^2 \csc^4 \theta \\ & + a^2 (a^2 + r^2) \left[a^2 (\bar{\mathcal{A}}_0^2 - \bar{\mathcal{A}}_1 \bar{\mathcal{A}}_2) - 2 \bar{\mathcal{A}}_0 \bar{\mathcal{A}}_5 + (\bar{\mathcal{A}}_0^2 - \bar{\mathcal{A}}_1 \bar{\mathcal{A}}_2) r^2 \right] \csc^2 \theta, \end{aligned} \quad (2.10)$$

and $\tilde{\Sigma}$ is given by Equation (1.8). The Kerr limit is now $\bar{\mathcal{A}}_5 \rightarrow \Delta$ while $\bar{\mathcal{A}}_{0,1,2} \rightarrow 1$.

The Johannsen limit is still $\bar{\mathcal{A}}_0^2 \rightarrow \bar{\mathcal{A}}_1 \bar{\mathcal{A}}_2$.

In order to map the CY metric with rescaled arbitrary functions, we solve for the $\bar{\mathcal{A}}_i$ functions as described at the end of Chapter 1. Then, we expand these rescaled functions about $r = \infty$, keep to second order in M/r as an example, and plug these

truncated expansions back into the rescaled CY metric. This is the CY reconstruction of beyond-GR metric X .

This rescaling of \mathcal{A}_5 functions by a factor of Δ was initially motivated by our analysis of Braneworld [21] and the rescaling by a factor of \mathcal{A}_5 was motivated by our analysis of Kerr-Sen [24]. Let us first look at the Braneworld case to understand the Δ rescaling. Both the numerator and denominator of the tt component of the CY metric mapped to Braneworld (using mapping functions exact in r) are proportional to Δ^2 , leading to a cancellation of Δ 's, and we therefore find no divergence at the Kerr horizon ($\Delta = 0$). Appendix A contains the mapping functions for Braneworld (and other considered metrics).

This Δ proportionality and cancellation breaks down when we expand the $\mathcal{A}_i(r)$ functions: the numerator of the tt component of CY mapped to Braneworld is proportional to Δ^0 while the denominator is proportional to Δ^2 . The tt component itself is then proportional to $\frac{1}{\Delta^2}$ and so we see a divergence at the Kerr horizon.

The idea is to factor Δ out of the $\mathcal{A}_i(r)$ functions themselves to cancel out the Δ in the denominator. This will therefore get rid of the divergence at the Kerr horizon. We show this cancellation for the $\mathcal{A}_5(r)$ function in the Braneworld example in Equations (2.11) and (2.12).

$$\mathcal{A}_{5Brane} = \frac{\Delta + \beta}{\Delta}, \quad (2.11)$$

$$\bar{\mathcal{A}}_{5Brane} = \left(\frac{\Delta + \beta}{\cancel{\Delta}} \right) \cancel{\Delta} = \Delta + \beta. \quad (2.12)$$

Now let us look at the Kerr-Sen case to understand why we also rescale by $\bar{\mathcal{A}}_5$. For the Kerr-Sen case, \mathcal{A}_2 is proportional to $1/\bar{\Delta}$ where $\bar{\Delta} = \Delta + 2br$, where b is the deviation parameter for the Kerr-Sen metric. \mathcal{A}_2 enters in the numerator of the tt component of the CY metric with the original parameterization, therefore there will be a divergence at $\bar{\Delta} = 0$. To remedy this, we must rescale by $\bar{\Delta}$: $\bar{\mathcal{A}}_5 = \bar{\Delta}$ for Kerr-Sen, so we rescale by the $\bar{\mathcal{A}}_5$ function.

In this rescaling scheme, we do not rescale the $f(r)$ function, we leave it as is. Note out of the six existing beyond-GR metrics we consider, $f(r)$ is only nonzero for Kerr-Sen.

2.2 Results and Discussion

In this section, we report the results of our attempt at removing the fictitious divergences through rescaling the arbitrary functions of r . Ideally, we want the CY metric to exactly recover the metric of each beyond-GR theory we consider, however, this is not always the case. To quantify how well the CY metric can recover metric X , we use a relative root-mean-square error (RMSE) calculation, given by

$$\text{RMSE} = \sqrt{\frac{\int_{r_{EH}}^{N r_{EH}} [g_{\alpha\beta}^X(r) - g_{\alpha\beta}^{CY}(r)]^2 dr}{\int_{r_{EH}}^{N r_{EH}} [g_{\alpha\beta}^X(r)]^2 dr}}. \quad (2.13)$$

Here, $g_{\alpha\beta}^X(r)$ is the “true” component from metric X and $g_{\alpha\beta}^{CY}(r)$ is the corresponding component from the CY metric with the rescaled mapping functions given by Equ-

tions (2.5) - (2.9). We integrate from the event horizon location of the beyond-GR theory we are considering, r_{EH} , to N event horizon distances, Nr_{EH} . We investigated the RMSE values for two different values of N : 2 and 100. We chose $2r_{EH}$ as an upper integration limit to get a sense of how well the CY metric can recover metric X near the horizon. Conversely, we chose $100r_{EH}$ as an upper integration limit to investigate how well the CY metric can recover X far from the horizon. We analyzed how the upper integration limit affects the RMSE and we found that the RMSE does not vary much with upper integration limits larger than $100r_{EH}$. This indicates that RMSEs integrated to $100r_{EH}$ give a good gauge on how well the CY metric can recover X for large distances. If the CY metric can exactly recover metric X , the RMSE value will be 0 – the closer the RMSE value is to 0, the better the performance of the CY metric.

The location of the event horizon, r_{EH} , of the CY metric will be different for each beyond-GR theory it is mapped to. The event horizon location can be calculated by equating the inverse of the rr component, $\frac{1}{g_{rr}}$, of CY mapped to metric X to 0, and solving for r . See Appendix A for event horizon locations for CY mapped to each of the six beyond-GR metrics considered in this work.

From this analysis we found the rescaling method successfully removes the fictitious divergences in the original CY metric, see Figure 2.1. Additionally, the CY metric with rescaling was able to recover Braneworld and Kalb-Ramond exactly. With the exception of the rr component of EdGB, the RMSE was less than 1.41×10^{-1} for

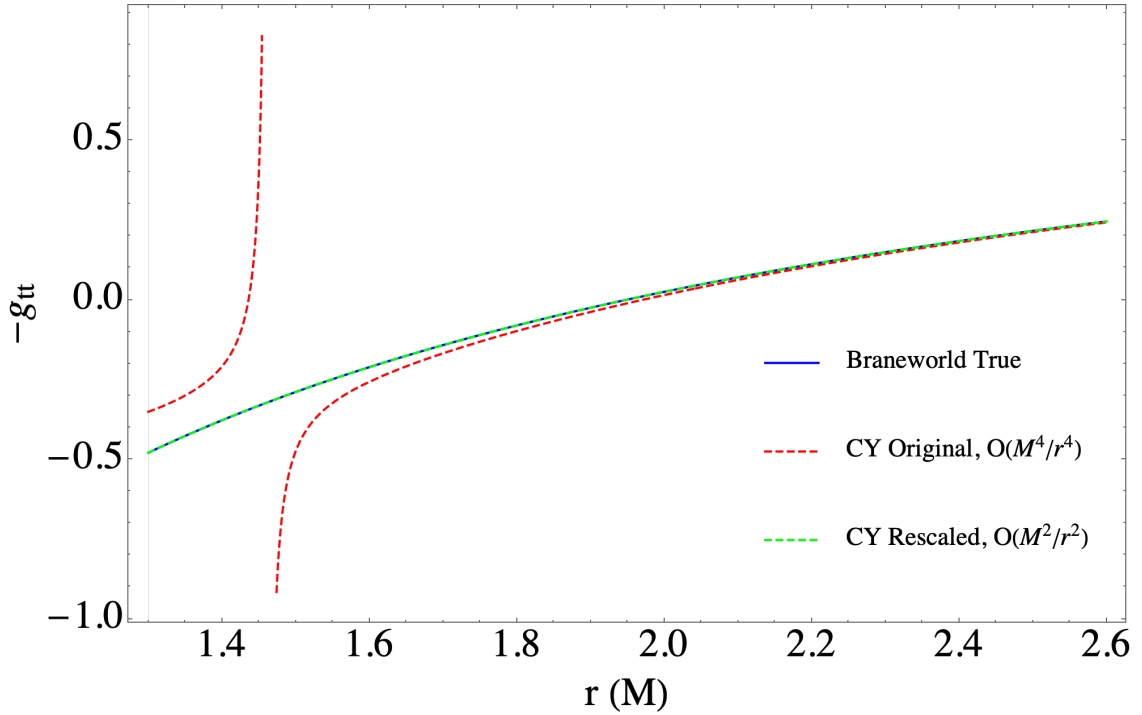


Figure 2.1: Similar to Figure 1.1 but with the result for the rescaled CY metric added. Notice that there is no longer a divergence in the rescaled CY metric which recovers the true Braneworld exactly. In this analysis, we again choose the parameter values $\theta = \frac{\pi}{2}$, $a = 0.9$, $M = 1$, and $\beta = 0.1$.

all components that CY could not recover exactly. The CY metric with the rescaling method has successfully reproduced the true metrics in most example theories.

Table 2.2 contains the relative RMSE value for each component of the CY metric mapped to the six metrics listed in Appendix A compared to the corresponding metric components of each beyond-GR metric. We choose parameter values of $M = 1$, $a = 0.9$, $\theta = \frac{\pi}{2}$, and the beyond-GR parameter for each set to 0.1 for these calculations.

Note RMSE calculations for dCS tt and rr components are not included in Table 2.2. This is because the $\bar{\mathcal{A}}_i$ functions present in those metric components are the same as those of Kerr, and so there is no possibility for deviation from Kerr to be present in these metric components. Additionally, EdGB and dCS do not have RMSE calculations for the $\phi\phi$ metric component. This is because the black hole spacetimes in these two theories that can be mapped to the CY metric are only valid to first order in spin, a . To account for this, we expanded the CY metric and kept to first order in a . This removed deviations from Kerr in the $\phi\phi$ component as the arbitrary functions of r are only seen in terms containing higher orders of a . And so we did not include this metric component in our analysis as it contains no deviations from Kerr and is therefore the same as Kerr for these theories.

Additionally, the rr component of the true EdGB metric diverges as it approaches the horizon. The rr component of the CY reconstruction of this theory also diverges as it approaches the horizon, but it does not diverge at the same rate as the true EdGB rr metric component. Because of this we set the lower integration limit in the RMSE calculation to be $1.01r_{EH}$ instead of the horizon distance so as to obtain a finite value for the RMSE. We also carried out the same analysis for the rr component of Bardeen because it exhibited a similar issue.

Note the CY metric with rescaling was unable to recover EdGB and dCS exactly when the $\bar{\mathcal{A}}_i$ functions were expanded and kept to second and fourth order in r , but it was able to exactly recover them when kept to sixth order. Figure 2.2 shows the EdGB

Metric	UIL [r_{EH}]	RMSE tt	RMSE rr	RMSE $\phi\phi$	RMSE $t\phi$
Braneworld	2	0	0	0	0
	100	0	0	0	0
Kerr-Sen	2	2.04×10^{-1}	0	4.50×10^{-2}	1.14×10^{-1}
	100	9.01×10^{-3}	0	5.09×10^{-6}	7.72×10^{-2}
		[23.65]	0	[14.75]	[2.78]
EdGB	2	8.83×10^{-2}	1.80	-	4.07×10^{-2}
	100	3.24×10^{-3}	1.69	-	2.84×10^{-2}
		[0]	[0]	-	[0]
dCS	2	-	-	-	1.20×10^{-2}
	100	-	-	-	8.46×10^{-3}
		-	-	-	[0]
Bardeen	2	1.13×10^{-4}	6.19×10^{-3}	2.79×10^{-6}	2.23×10^{-5}
	100	2.37×10^{-6}	5.30×10^{-3}	2.02×10^{-10}	1.58×10^{-5}
		$[5.72 \times 10^{-11}]$	$[1.67 \times 10^{-7}]$	$[4.88 \times 10^{-15}]$	$[3.81 \times 10^{-10}]$
Kalb-Ramond	2	0	0	0	0
	100	0	0	0	0

Table 2.1: RMSE for each component of the CY metric compared to the corresponding beyond-GR metric given in the “Metric” column. UIL denotes upper integration limit in the RMSE calculation in units of event horizons. Dashes denote components that have no deviation from Kerr. Values in square brackets are RMSE values for \mathcal{A}_i expanded to 6th order with UIL $100r_{EH}$.

tt component as an example of this – keeping to higher orders in the expansion in r causes the CY metric to better approximate and eventually recover the true metric.

From Table 2.2, we see a new divergence is introduced to CY mapped to Kerr-Sen when the $\bar{\mathcal{A}}_i$ functions are expanded and kept to sixth order in r . In Figure 2.3, we show the true tt component of Kerr-Sen compared to the tt component of the CY metric with original mapping, the CY metric with rescaling kept to second, fourth, and sixth order in r , and the CY metric with the small deviation approximation detailed in Chapter 3. We can see the divergence in the original mapping of the CY metric, the red dashed curve. Both the rescaling method and the small deviation approximation remove that divergence. However, we do see the CY metric with rescaling exhibits a new divergence at sixth order in the expansion about $r = \infty$. This divergence occurs at $r = 1.06$. We plan to study what causes this divergence to emerge at this order and why the emergence of this new divergence is dependent upon the order kept in the r expansion.

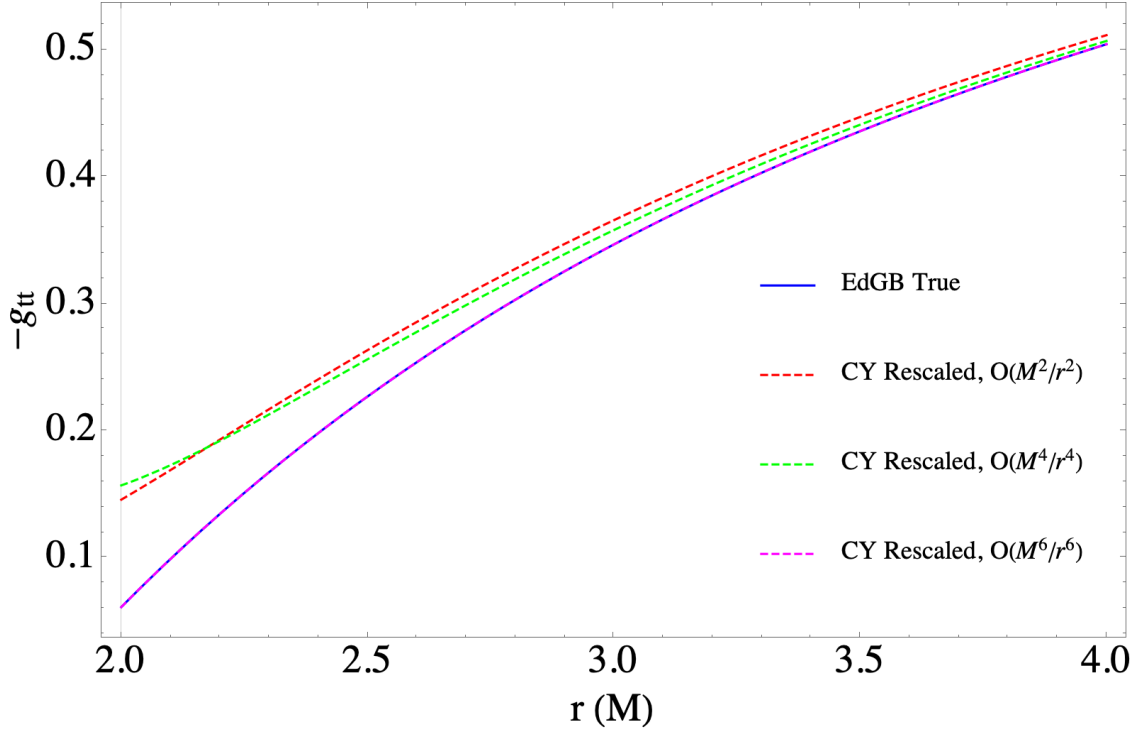


Figure 2.2: The tt component of the metric for the true EdGB black hole (blue solid) and the rescaled CY metric with $\bar{\mathcal{A}}_i$ expanded to various orders (dashed). The CY tt metric component expanded to orders $\frac{M^2}{r^2}$ and $\frac{M^4}{r^4}$ do not agree well with the true EdGB metric component. There is more disagreement near the horizon and the CY metric component approaches the true EdGB as the radial distance increases. The CY tt metric component expanded to order $\frac{M^6}{r^6}$ recovers the true EdGB metric component exactly. We choose parameter values $\theta = \frac{\pi}{2}$, $a = 0.9$, $M = 1$, and $\beta = 0.1$.

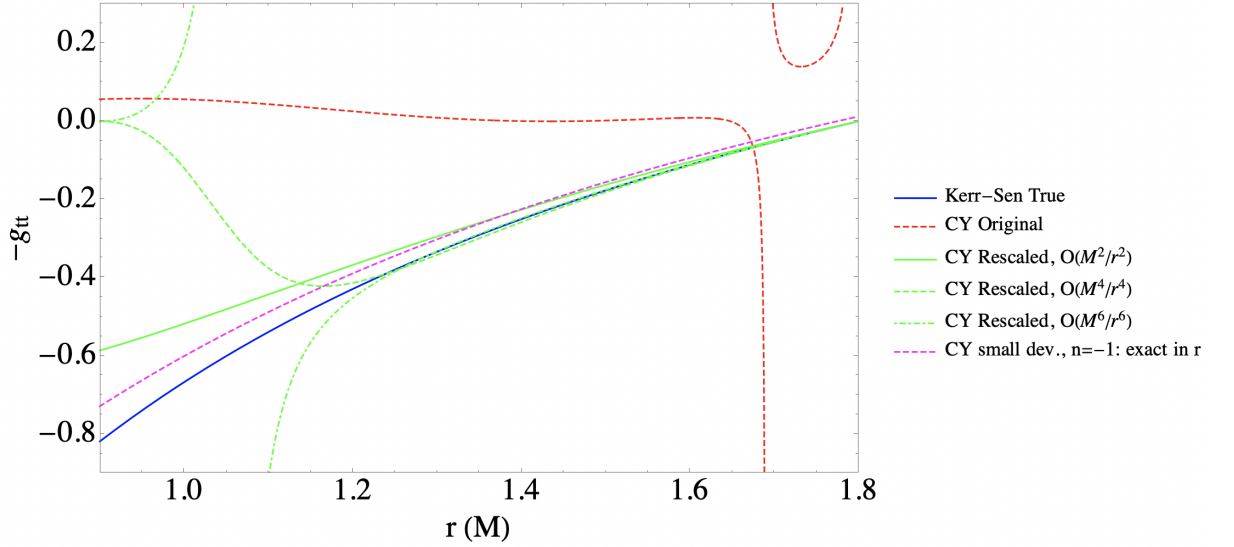


Figure 2.3: The tt component for the true Kerr-Sen black hole (blue solid), the CY metric with original mapping (red dashed), the rescaled CY metric to second order (green solid), fourth order (green dashed), and sixth order (green dash-dotted), and the CY metric with small deviation approximation with $n = -1$ exact in r (magenta dashed). All rescaled CY and CY with small deviation approximation remove divergence seen in original CY. A new divergence emerges for rescaled CY expanded to sixth order. We choose parameter values $\theta = \frac{\pi}{2}$, $a = 0.9$, $M = 1$, and $b = 0.1$.

Chapter 3

Small Deviation Approximation

The fictitious divergence seen in the original CY metric by using the truncated \mathcal{A}_i functions arises because of the non-Kerr contribution in the denominators of each metric component. Therefore, in this chapter, we attempt to remove the nonphysical divergence by assuming that the deviations from Kerr are small and treat them as small perturbations. The spirit is similar to what was already done in [25] that constructed non-Kerr spacetimes preserving Kerr symmetries under small deviation from Kerr. We split the \mathcal{A}_i functions into Kerr plus correction instead of parameterizing the \mathcal{A}_i functions themselves. We performed this split as follows: $\mathcal{A}_i = 1 + \epsilon \Delta^n \delta \mathcal{A}_i$ with parameters $\delta \mathcal{A}_i$ and n . Here, ϵ is a bookkeeping parameter that we use to count the order of deviation from Kerr. Below, Approach 1 refers to $n = -1$, Approach 2 refers to $n = 0$, and Approach 3 refers to $n = 1$.

In addition to the \mathcal{A}_i functions, we parameterize the $f(r)$ function and perform

similar expansions as we did for \mathcal{A}_i . It takes a slightly different form, $f(r) = \epsilon\Delta^n\delta f(r)$, as its Kerr limit is 0. Note, $f(r) = 0$ for all beyond-GR metrics we considered except Kerr-Sen.

To summarize, we list the forms of the small deviation approximation parameterization here:

$$\mathcal{A}_i = 1 + \epsilon\Delta^n\delta\mathcal{A}_i, \quad (3.1)$$

$$f(r) = \epsilon\Delta^n\delta f(r), \quad (3.2)$$

where n takes the value of either $-1, 0$, or 1 for the analyses below. Notice that if we use the full expression for $\delta\mathcal{A}_i$, the results are the same for any n . The difference in n becomes important when we use $\delta\mathcal{A}_i$ expanded about $r = \infty$. We will expand the metric about $\epsilon = 0$ and only keep to linear order. Here we do not explicitly show the expression for the the small deviation approximation CY metric as the expression itself is quite long.

3.1 Finding $\delta\mathcal{A}_i$ Mappings

The process for finding the $\delta\mathcal{A}_i$ mappings begins with finding the \mathcal{A}_i mapping functions for metric X in the same way as described in Section 1.2. Once we have the \mathcal{A}_i mappings, which are a function of the beyond-Kerr parameters of metric X , we expand them about a small deviation from Kerr. We then equate this expanded \mathcal{A}_i function to the particular parameterization form we are considering, $1 + \epsilon\Delta^n\delta\mathcal{A}_i$ with

ϵ set to 1 and n being either -1, 0, or 1, and solve for $\delta\mathcal{A}_i$. This $\delta\mathcal{A}_i$ function is what we will refer to as the “exact” mapping, as it is exact in r . We also expand $\delta\mathcal{A}_i$ about $r = \infty$ and kept to sixth order, for example. This is what we will refer to as the “expanded” mapping, as these $\delta\mathcal{A}_i$ are not exact in r .

Next we plug either the exact or expanded $\delta\mathcal{A}_i$ mapping back into the CY metric that has been expanded about $\epsilon = 0$ and kept to linear order in ϵ . We treat the expansion of the rr component differently than the other components. We first take the inverse of the rr component, then expand in ϵ and keep to first order, then take the inverse again. This is to account for nonlinear contributions in ϵ .

For each Approach 1, 2, and 3, we found both the exact and expanded $\delta\mathcal{A}_i$ mappings of the CY metric to each of the six chosen metrics and listed them in Appendix A. We quantified how well the CY reconstructions of these metrics were able to recover each existing beyond-GR metric with a similar RMSE analysis as done in Section 2.2.

3.2 Results and Discussion

In this section, we report the results of our attempt to remedy the fictitious divergences seen in the original CY parameterization with the small deviation approximation. We find CY with $\delta\mathcal{A}_i$ exact in r removes the fictitious divergences seen in the original CY metric parameterization for all three Approaches ($n = -1, 0, 1$).

We also report the RMSE values quantifying the CY metric’s ability to recover the six beyond-GR metrics we considered. We calculated the RMSE for each metric

component of CY mapped to each of the six existing beyond-GR metrics considered for the three Approaches of n with either the exact or expanded $\delta\mathcal{A}_i$ mappings. Like in the rescaled attempt, we considered two different upper integration limits, $2r_{EH}$ and $100r_{EH}$ in our RMSE analysis. In the tables below, the column denoted “UIL” still stands for upper integration limit and is again in units of r_{EH} .

Tables 3.1, 3.2, and 3.3 show the values of the RMSE for the components of CY mapped to each beyond-GR metric that are the largest – out of the tt , rr , $t\phi$, and $\phi\phi$ (where applicable) metric components, we report the component that had the largest RMSE. The component that corresponds to this maximum value is given in parenthesis next to the RMSE value. In this attempt, we calculated quite a few RMSE values, so for brevity and clarity, we only report the maximum errors as they give insight as to where the CY metric is performing the worst. Table 3.1 gives the maximum RMSE values for Approach 1 ($n = -1$), Table 3.2 gives the maximum RMSE values for Approach 2 ($n = 0$), and Table 3.3 gives the maximum RMSE values for Approach 3 ($n = 1$). The RMSE values were calculated using Equation (2.13) with specific parameter values of $M = 1$, $a = 0.9$, $\theta = \frac{\pi}{2}$, and the beyond-GR parameter for each set to 0.1. Let us discuss below the results for each Approach in more detail.

Maximum RMSE Values: Approach 1 (n = -1)			
Metric	UIL [r_{EH}]	Exact	Expanded
Braneworld	2	0	-
	100	0	-
Kerr-Sen	2	1.01×10^{-1} (tt)	28.7 (tt)
	100	2.08×10^{-2} (tt)	1.42 ($t\phi$)
EdGB	2	0	1.50 (rr)
	100	0	1.50 (rr)
dCS	2	0	14.50 ($t\phi$)
	100	0	2.72 ($t\phi$)
Bardeen	2	1.13×10^{-4} (tt)	1.13×10^{-4} (tt)
	100	2.23×10^{-5} ($t\phi$)	2.23×10^{-5} ($t\phi$)
Kalb-Ramond	2	0	0
	100	0	0

Table 3.1: Table of maximum RMSE values for each metric with CY small deviation approximation parameteriation for Approach 1 ($n = -1$). dCS has a divergence in this approach, hence the large RMSE value. The $\delta\mathcal{A}_i$ for Braneworld does not depend on r ; dashes indicate that there is no expanded $\delta\mathcal{A}_i$.

Maximum RMSE Values: Approach 2 ($n = 0$)			
Metric	UIL [r_{EH}]	Exact	Expanded
Braneworld	2	0	1.28×10^{-1} (tt)
	100	0	1.77×10^{-2} ($t\phi$)
Kerr-Sen	2	1.01×10^{-1} (tt)	1.96×10^1 (tt)
	100	2.08×10^{-2} (tt)	6.91×10^{-2} ($t\phi$)
EdGB	2	0	1.01 (rr)
	100	0	1.01 (rr)
dCS	2	0	0
	100	0	0
Bardeen	2	1.51×10^{-5} (tt)	2.00×10^{-3} (tt)
	100	4.60×10^{-6} ($t\phi$)	6.09×10^{-4} ($t\phi$)
Kalb-Ramond	2	0	2.11×10^{-1} (tt)
	100	0	3.04×10^{-2} ($t\phi$)

Table 3.2: Table of maximum RMSE values for each metric with CY small deviation approximation parameteriation for Approach 2 ($n = 0$).

Maximum RMSE Values: Approach 3 ($n = 1$)			
Metric	UIL [r_{EH}]	Exact	Expanded
Braneworld	2	0	1.41×10^{-1} (tt)
	100	0	1.95×10^{-2} ($t\phi$)
Kerr-Sen	2	1.01×10^{-1} (tt)	26.5 (rr)
	100	2.08×10^{-2} (tt)	26.5 (rr)
EdGB	2	0	1.02 (rr)
	100	0	1.02 (rr)
dCS	2	0	3.89×10^{-3} ($t\phi$)
	100	0	2.76×10^{-3} ($t\phi$)
Bardeen	2	1.51×10^{-5} (tt)	4.63×10^{-3} (tt)
	100	2.23×10^{-5} ($t\phi$)	1.42×10^{-3} ($t\phi$)
Kalb-Ramond	2	0	2.12×10^{-1} (tt)
	100	0	3.40×10^{-2} ($t\phi$)

Table 3.3: Table of maximum RMSE values for each metric with CY small deviation approximation parameteriation for Approach 3 ($n = 0$).

3.2.1 Approach 1: $n = -1$

The CY metric with the $\delta\mathcal{A}_i$ mapping exact in r exactly recovers four out of the six beyond-GR metrics we considered: Braneworld, EdGB, dCS, and Kalb-Ramond. Also, as mentioned above, the exact mapping removes the nonphysical divergence seen in the original CY parameterization, see Figure 3.1 for the Braneworld tt component example. From this figure, we can see that the CY metric tt component with the exact parameterization in Approach 1 no longer shows a divergence at the Kerr horizon. Let us discuss this example to understand why this divergence goes away for Approach 1 with the exact mapping. The denominator of the tt component of the CY metric for Approach 1 is proportional to Δ^2 . The $\delta\mathcal{A}_i$ mappings are constant in r . The specific combination of $\delta\mathcal{A}_i$ multiplied by Δ 's in the numerator lead to a cancellation of the Δ^2 in the denominator, and thus we see no divergence at the Kerr horizon. Despite its ability to exactly recover the Braneworld, EdGB, dCS, and Kalb-Ramond, Approach 1 with exact $\delta\mathcal{A}_i$ was unable to recover Kerr-Sen and Bardeen exactly; the RMSE values for those metrics are all less than 1.01×10^{-1} .

Approach 1 with the expanded $\delta\mathcal{A}_i$ successfully removes divergences for the Bardeen and Kalb-Ramond metrics. It still shows divergences at the Kerr horizon for Kerr-Sen, EdGB, and dCS. We see these divergences as large RMSE values in Table 3.1. Let us look at the $t\phi$ component of the CY metric mapped to dCS more in depth, similarly to how we did above with Braneworld, as an example to understand why this divergence comes about with the mappings expanded in r . The numerator of the

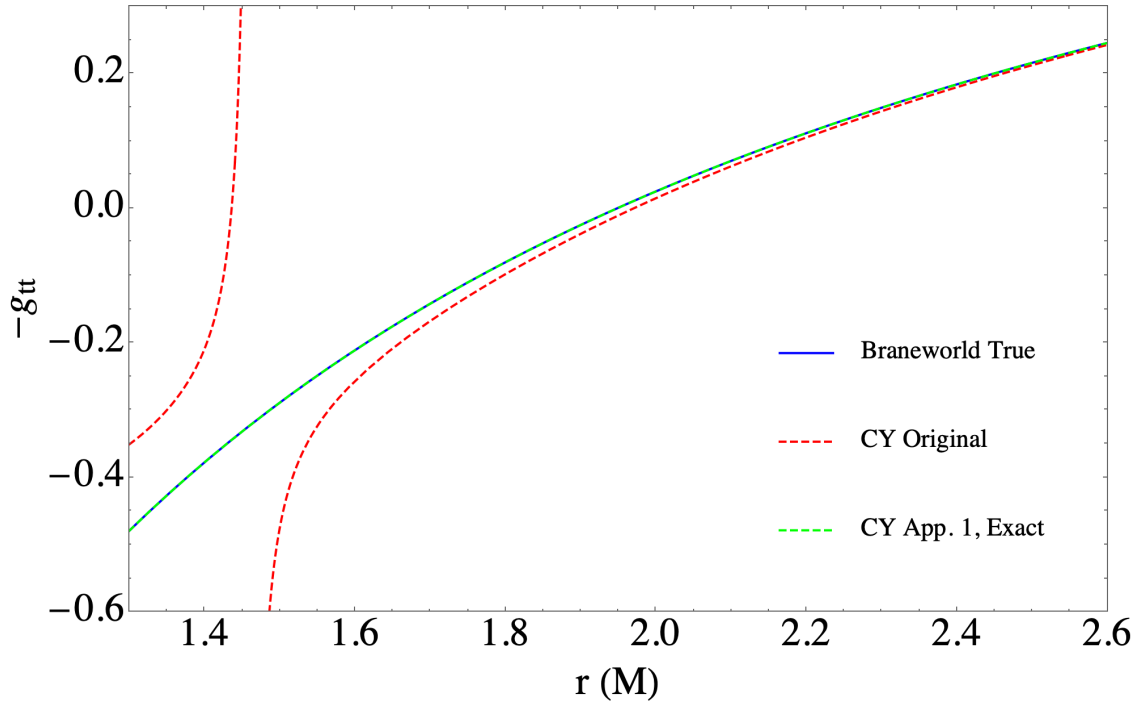


Figure 3.1: Similar to Figure 1.1 but with the result for the small deviation CY metric for Approach 1 ($n = -1$) added. The small deviation CY metric successfully removed the fictitious divergence and recovered the true Braneworld black hole metric exactly. Note there is no expanded parameterization for Approach 1 because the mapping functions $\delta\mathcal{A}_i$ are independent of r . In this analysis we choose parameter values $\theta = \frac{\pi}{2}$, $a = 0.9$, $M = 1$, and $\beta = 0.1$.

CY metric here is proportional to $\frac{1}{\Delta}$ to first order in spin (the dCS metric that can be mapped to CY is only valid to first order in spin). $\delta\mathcal{A}_i$ exact in r for this Approach are proportional to Δ , again to first order in spin. This leads to a cancellation of Δ 's and therefore we see no divergence. The expanded $\delta\mathcal{A}_i$ for this Approach, however, are proportional to Δ^0 . This means we no longer get a cancellation of Δ 's and so the $t\phi$ component of the CY metric is proportional to $\frac{1}{\Delta}$ and we see a divergence at the Kerr horizon. Figure 3.2 shows this remaining nonphysical divergence in the dCS example. We see divergences in Kerr-Sen and EdGB for the expanded mappings for a similar reason.

The CY metric with the expanded $\delta\mathcal{A}_i$ mapping recovers Kalb-Ramond exactly. It did not recover Kerr-Sen, EdGB, dCS, and Bardeen exactly.

3.2.2 Approach 2: $n = 0$

The CY metric with $\delta\mathcal{A}_i$ mappings exact in r for this Approach exactly recovers the same four beyond-GR metrics as Approach 1: Braneworld, EdGB, dCS, and Kalb-Ramond. As mentioned in Section 3.2, the CY metric with Approach 2 exact $\delta\mathcal{A}_i$ parameterization removes the fictitious divergence seen with the CY original parameterization. Let us go through a similar reasoning as we did for Approach 1 to understand why this parameterization removes the original CY divergence. The denominator of the tt component of the CY metric with the Approach 2 exact parameterization is proportional to Δ . The Braneworld $\delta\mathcal{A}_i$ mappings are proportional to

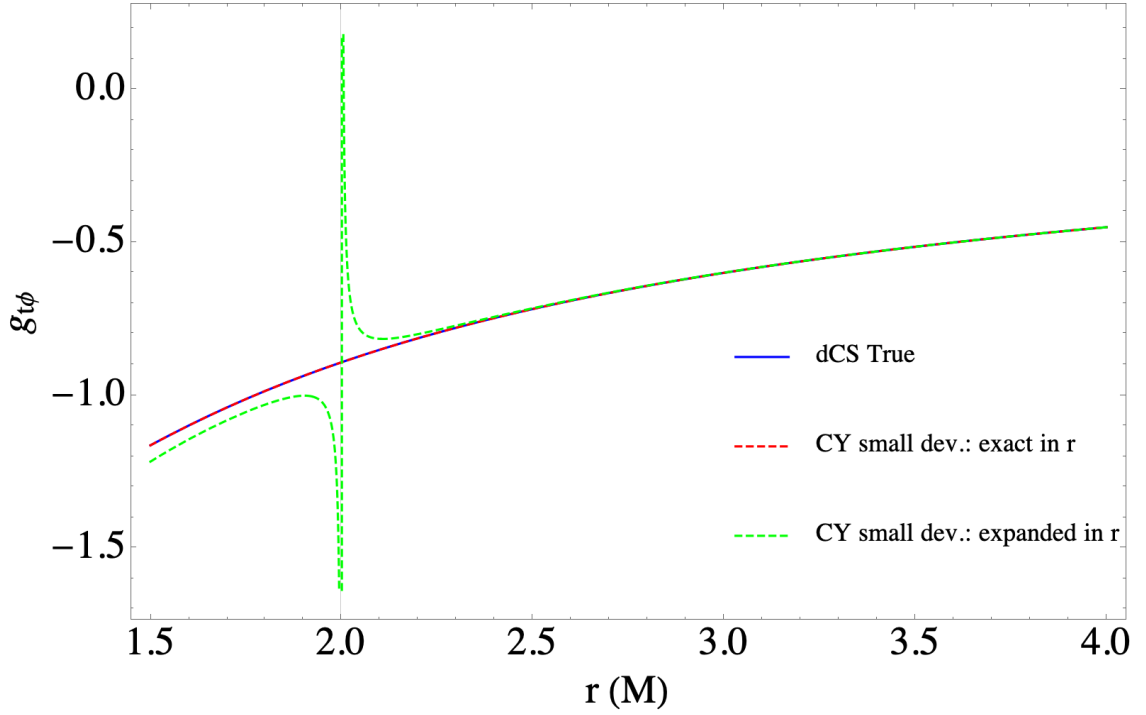


Figure 3.2: Nonphysical divergence seen in the expanded mapping of Approach 1 ($n = -1$) for the $t\phi$ component of the CY metric mapped to dCS. The true dCS $t\phi$ metric component is shown as the blue solid line, the CY $t\phi$ metric component mapped to dCS with the exact Approach 1 mapping is shown as the red-dashed line, and the CY $t\phi$ metric component mapped to dCS with the expanded Approach 1 mapping is shown as the green-dashed line. We see a nonphysical divergence at $r = 2M$. In this analysis we choose parameter values $\theta = \frac{\pi}{2}$, $a = 0.9$, $M = 1$, and $\zeta = 0.1$.

$\frac{1}{\Delta}$. This leads to an overall $\frac{1}{\Delta^2}$ that cancels out with the Δ^2 seen in the numerator of the CY tt component, thus resulting in no divergence at the Kerr horizon. Figure 3.3 gives a visualization of this divergence remedy in this example and highlights that the Braneworld metric is recovered exactly with the exact $\delta\mathcal{A}_i$ parameterization of CY in this Approach. From this Figure, we also note that the expanded parameterization with $n = 0$ also removes the original CY divergence. Let us now discuss the CY metric with the $\delta\mathcal{A}_i$ mappings expanded in r .

The CY metric with the expanded $\delta\mathcal{A}_i$ mappings is unable to exactly recover any of the six beyond-GR metrics we considered, but all RMSE values are below 1.96×10^{-1} . It is important to note that we do not see new divergences emerge in the CY metric here like we did in Approach 1. In Table 3.2, the RMSE for the rr component of EdGB indicates a divergence because of its large value. The rr component of the true EdGB metric itself diverges near the horizon. Similar to Approach 1, the CY reconstruction of the EdGB metric for this Approach 2 also diverges near the horizon, but at a slightly different rate than that of true EdGB. This causes the large RMSE value, but is not in fact a new or fictitious divergence.

The CY metric with the exact Approach 2 mappings does not exactly recover the Kerr-Sen and Bardeen metrics, however they both have small RMSE values below 1.01×10^{-1} .

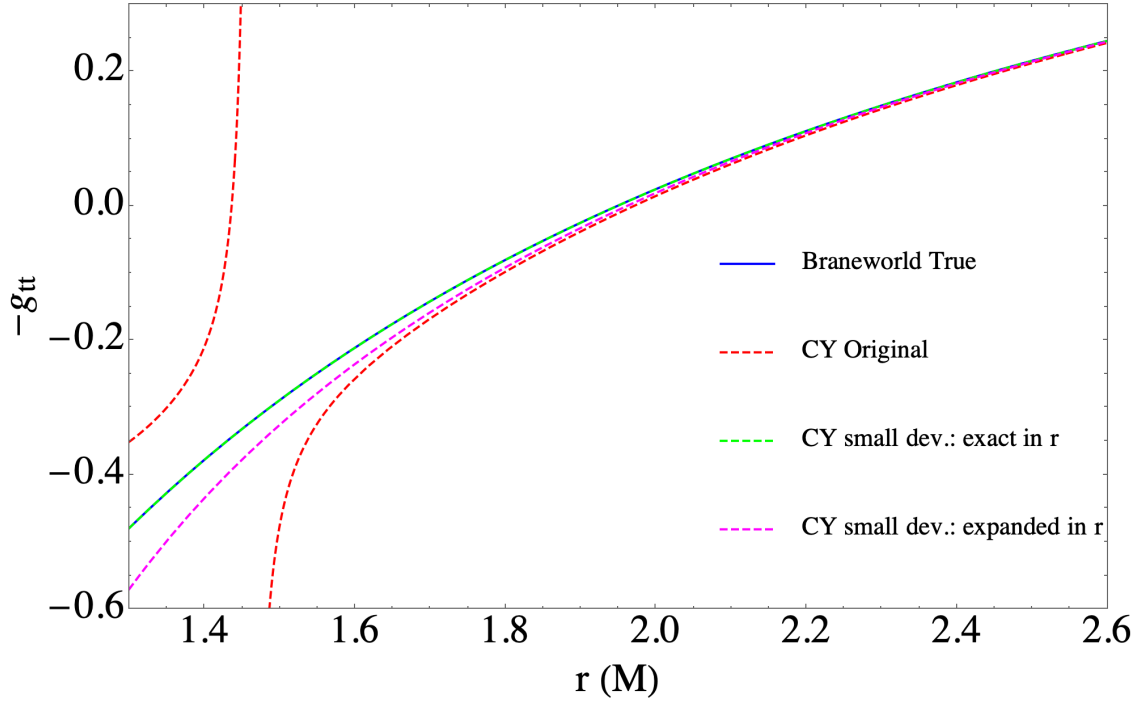


Figure 3.3: Similar to Figure 3.1 but for Approach 2 ($n = 0$). Both the exact and expanded Approach 2 parameterizations successfully removed the fictitious divergence. The exact parameterization recovered the true Braneworld metric exactly while the expanded version approaches the true metric as r increases. Again we choose parameter values $\theta = \frac{\pi}{2}$, $a = 0.9$, $M = 1$, and $\beta = 0.1$.

3.2.3 Approach 3: $n = 1$

Like both Approach 1 and 2, Approach 3 with $\delta\mathcal{A}_i$ exact in r exactly recovers the same four beyond-GR metrics: Braneworld, EdGB, dCS, and Kalb-Ramond. This parameterization was unable to recover Kerr-Sen and Bardeen exactly, and both have RMSE values below 1.01×10^{-2} . As mentioned earlier, the exact $\delta\mathcal{A}_i$ mappings for Approach 3 remove the fictitious divergence seen in the original CY metric parameterization. We can see this in Figure 3.4 again for the Braneworld tt example. Following a similar analysis as Sections 3.2.1 and 3.2.2, let us look at how this divergence is removed by the exact $\delta\mathcal{A}_i$ parameterization. The denominator of the tt component of the CY metric with $\delta\mathcal{A}_i$ exact in r with $n = 1$ is proportional to Δ^0 . The Braneworld $\delta\mathcal{A}_i$ mapping functions are proportional to $\frac{1}{\Delta^2}$ are canceled by the Δ^2 in the numerator of the tt component, leading to no divergence at the Kerr horizon.

From Table 3.3, we again see the RMSE of the rr component of CY reconstruction of EdGB with the expanded $\delta\mathcal{A}_i$ mapping is large. This again is due to the different rates of divergence in both the true and CY metric components; it is not a new or nonphysical divergence. We do, however, see a new divergence emerge for CY mapped to Kerr-Sen expanded in r at the Kerr horizon. Let us take a look at why this divergence emerges in the expanded parameterization but not in the exact parameterization. In the exact case, the denominator of the rr component of the CY metric with $n = 1$ parameterization is proportional to Δ^2 . $\delta\mathcal{A}_5$ is in the denominator of the rr component and is the only mapping function that enters in this component.

$\delta\mathcal{A}_5$ is proportional to $\frac{1}{\Delta^2}$, which leads to a complete cancellation of Δ s in the denominator and thus there is no divergence at the Kerr horizon for Approach 3 exact in r . When we expand $\delta\mathcal{A}_5$ about $r = \infty$, it loses its $\frac{1}{\Delta^2}$ form, and so there is no Δ cancellation in the denominator, leading to a divergence at the Kerr horizon.

3.3 Summary

Approaches 2 and 3 were able to remove the fictitious divergences seen in the original CY metric parameterization for all six beyond-GR metrics considered here. Approach 1 was able to remove this fictitious divergence for all beyond-GR metrics except the $t\phi$ component of the dCS metric.

Approach 3 ($n = 0$) performs best (has the lowest RMSE values) for EdGB, dCS, and Kerr-Sen. Approach 1 ($n = -1$) performs best (has the lowest RMSE values) for Braneworld, Bardeen, and Kalb-Ramond.

It is important to note that the new divergences we saw emerge in the expanded mappings of Approach 1 and 3 appear when we choose a high spin, $a = 0.9$. These new divergences do not appear for small spin like $a = 0.3$, for example. This will require further study to understand why these divergences emerge for high spin.

Recall for these RMSE calculations, we chose specific parameter values for $\theta = \frac{\pi}{2}$, $a = 0.9$, $M = 1$, and set the beyond-GR parameters to 0.1 in the mapping functions and metric components. For each Approach 1, 2, and 3, we also varied a and θ and determined which values of a and θ yield the largest RMSE value for the CY

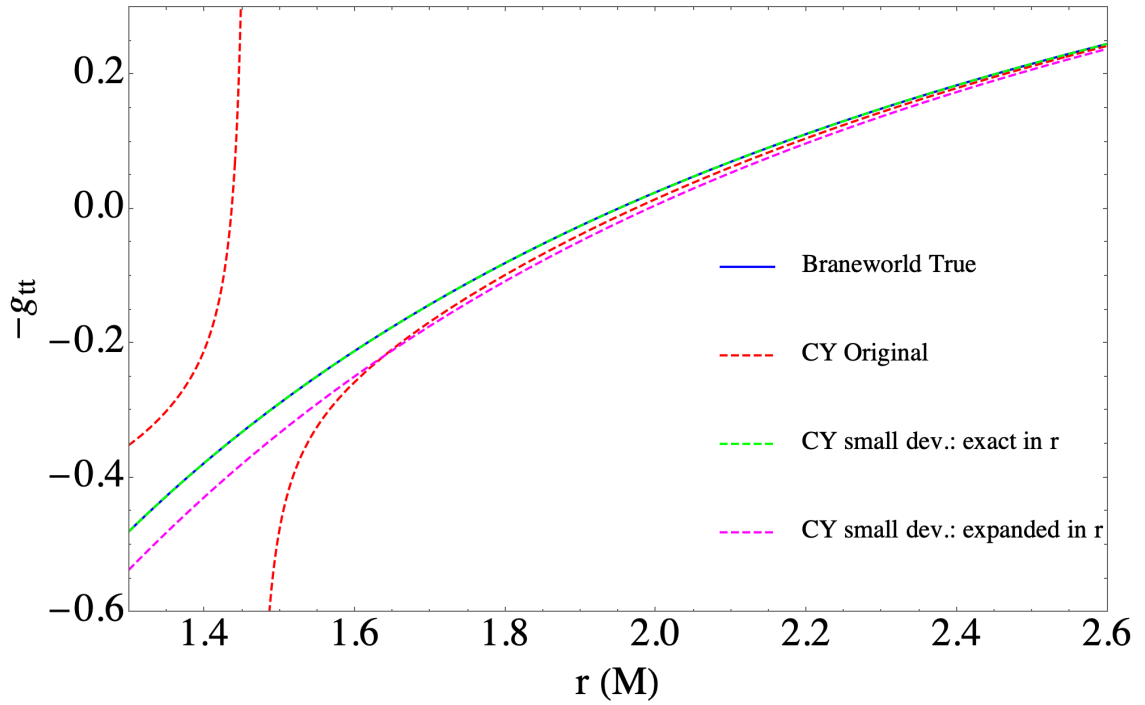


Figure 3.4: Similar to Figure 3.1 but for Approach 3 ($n = 1$). Like Approach 2, both the exact and expanded Approach 3 parameterizations successfully removed the fictitious divergence. The exact parameterization recovered the true Braneworld metric exactly while the expanded one approaches the true metric as r increases. We choose parameter values $\theta = \frac{\pi}{2}$, $a = 0.9$, $M = 1$, and $\beta = 0.1$.

reconstruction of the Braneworld metric. See Appendix B for a summary of these calculations. Based on this analysis, $\theta = 2.61304$ and $a = 0.918921$ give the maximum RMSE for the tt , rr , and $t\phi$ components of the CY metric mapped to Braneworld and $\theta = 1.79845$ and $a = 0.896642$ give the maximum RMSE for the $\phi\phi$ component.

Chapter 4

Conclusion

The goal of this work was to refine the CY metric presented in [20] to remove pathological behaviors including nonphysical divergences. We took two different attempts to remedy this pathology: rescaling the CY \mathcal{A}_i mapping functions, and making a small deviation approximation with three different approaches. We successfully eliminated the existing pathological behavior when mapping the CY metric to six beyond-GR metrics with the rescaling attempt and Approaches 2 and 3 of the small deviation approximation attempt. A nonphysical divergence was still seen in the CY metric mapped to dCS and Kerr-Sen in Approach 1 of the small deviation approximation, but CY metric exhibited no such pathologies when mapped to the other four metrics we considered.

The CY metric with the rescaled \mathcal{A}_i functions detailed in Chapter 2 was able to recover the Braneworld and Kalb-Ramond metrics exactly and outperformed the small

deviation approximation detailed in Chapter 3 for the Kerr-Sen and EdGB metrics. It comes very close to the small deviation approximation for Bardeen metric; we prefer the rescaling method for Bardeen to the small deviation approximation because it performs almost as well while not assuming that the deviation from Kerr is small.

The CY metric with the small deviation approximation Approach 2 with $n = 0$ parameterization performed the best for dCS as it was able to recover the metric exactly. This may be due to that the small coupling approximations in the dCS metric.

The rescaled CY metric was able to remove the divergence in the original CY metric for the example theories studied here except for the Kerr-Sen black hole, where the diverging behavior is still present when the expansion for $\bar{\mathcal{A}}_i$ at higher orders. The divergence is not at the Kerr horizon or the true horizon (this was cured by our rescaling), but arises because the denominator in the metric component can vanish at some other points that depend on how many terms one keeps in the expansion of the mapping functions. To remedy this further, one possibility is to combine the two refinements we performed. Namely, we first carry out the rescaling, and then apply the small deviation approximation. The latter will ensure that we will no longer have divergence, though the approximate metric may not recover well the true one if non-linear effects due to non-Kerr effects are large. Taking Kerr-Sen as an example, the non-Kerr parameter b enters both in the numerator and denominator of the mapping functions \mathcal{A}_i for the original CY metric while b only enters in the

numerator of $\bar{\mathcal{A}}_i$ for the rescaled CY metric, up to second order in b . This implies that the rescaled mapping functions are simpler and have smaller nonlinear effects in terms of deviations from Kerr. This could be an interesting avenue for future work.

Bibliography

- [1] Clifford M. Will. The Confrontation between General Relativity and Experiment. *Living Rev. Rel.*, 17:4, 2014. doi: 10.12942/lrr-2014-4.
- [2] C. M. Will. *Theory and Experiment in Gravitational Physics*. Cambridge University Press, Cambridge, UK, March 1993.
- [3] Ingrid H. Stairs. Testing general relativity with pulsar timing. *Living Rev.Rel.*, 6:5, 2003.
- [4] Norbert Wex. Testing Relativistic Gravity with Radio Pulsars. 2014.
- [5] Bhuvnesh Jain and Justin Khoury. Cosmological tests of gravity. *Annals of Physics*, 325(7):1479–1516, July 2010. doi: 10.1016/j.aop.2010.04.002.
- [6] Austin Joyce, Bhuvnesh Jain, Justin Khoury, and Mark Trodden. Beyond the Cosmological Standard Model. *Phys. Rept.*, 568:1–98, 2015. doi: 10.1016/j.physrep.2014.12.002.

- [7] Kazuya Koyama. Cosmological tests of modified gravity. *Reports on Progress in Physics*, 79(4):046902, April 2016. doi: 10.1088/0034-4885/79/4/046902.
- [8] Werner Israel. Event horizons in static vacuum space-times. *Phys. Rev.*, 164: 1776–1779, 1967. doi: 10.1103/PhysRev.164.1776.
- [9] S. W. Hawking. Black holes in general relativity. *Commun. Math. Phys.*, 25: 152–166, 1972. doi: 10.1007/BF01877517.
- [10] Dimitrios Psaltis et al. Gravitational Test Beyond the First Post-Newtonian Order with the Shadow of the M87 Black Hole. *Phys. Rev. Lett.*, 125(14):141104, 2020. doi: 10.1103/PhysRevLett.125.141104.
- [11] Dimitrios Psaltis, Colm Talbot, Ethan Payne, and Ilya Mandel. Probing the Black Hole Metric. I. Black Hole Shadows and Binary Black-Hole Inspirals. *Phys. Rev. D*, 103:104036, 2021. doi: 10.1103/PhysRevD.103.104036.
- [12] Clifford M. Will. Testing the general relativistic “no-hair” theorems using the galactic center black hole sagittarius a*. *The Astrophysical Journal*, 674(1):L25, jan 2008. doi: 10.1086/528847. URL <https://dx.doi.org/10.1086/528847>.
- [13] David Merritt, Tal Alexander, Seppo Mikkola, and Clifford M. Will. Testing Properties of the Galactic Center Black Hole Using Stellar Orbits. *Phys. Rev. D*, 81:062002, 2010. doi: 10.1103/PhysRevD.81.062002.
- [14] Laleh Sadeghian and Clifford M. Will. Testing the black hole no-hair theorem at

- the galactic center: Perturbing effects of stars in the surrounding cluster. *Class. Quant. Grav.*, 28:225029, 2011. doi: 10.1088/0264-9381/28/22/225029.
- [15] R. Abbott et al. Tests of general relativity with binary black holes from the second LIGO-Virgo gravitational-wave transient catalog. *Phys. Rev. D*, 103(12):122002, 2021. doi: 10.1103/PhysRevD.103.122002.
- [16] Collin D. Capano, Miriam Cabero, Julian Westerweck, Jahed Abedi, Shilpa Kasta, Alexander H. Nitz, Alex B. Nielsen, and Badri Krishnan. Observation of a multimode quasi-normal spectrum from a perturbed black hole. *arXiv e-prints*, art. arXiv:2105.05238, May 2021.
- [17] Maximiliano Isi, Matthew Giesler, Will M. Farr, Mark A. Scheel, and Saul A. Teukolsky. Testing the no-hair theorem with GW150914. *Phys. Rev. Lett.*, 123(11):111102, 2019. doi: 10.1103/PhysRevLett.123.111102.
- [18] Tim Johannsen. Regular Black Hole Metric with Three Constants of Motion. *Phys. Rev. D*, 88(4):044002, 2013. doi: 10.1103/PhysRevD.88.044002.
- [19] Roman Konoplya, Luciano Rezzolla, and Alexander Zhidenko. General parametrization of axisymmetric black holes in metric theories of gravity. *Phys. Rev. D*, 93(6):064015, 2016. doi: 10.1103/PhysRevD.93.064015.
- [20] Zack Carson and Kent Yagi. Asymptotically flat, parametrized black hole metric preserving kerr symmetries. *Physical Review D*, 101(8), Apr 2020. ISSN 2470-

0029. doi: 10.1103/physrevd.101.084030. URL <http://dx.doi.org/10.1103/PhysRevD.101.084030>.
- [21] A. N. Aliev and A. E. Gumrukcuoglu. Charged rotating black holes on a 3-brane. *Phys. Rev. D*, 71:104027, 2005. doi: 10.1103/PhysRevD.71.104027.
- [22] Lisa Randall and Raman Sundrum. A Large mass hierarchy from a small extra dimension. *Phys. Rev. Lett.*, 83:3370–3373, 1999. doi: 10.1103/PhysRevLett.83.3370.
- [23] Lisa Randall and Raman Sundrum. An Alternative to compactification. *Phys.Rev.Lett.*, 83:4690–4693, 1999. doi: 10.1103/PhysRevLett.83.4690.
- [24] Ashoke Sen. Rotating charged black hole solution in heterotic string theory. *Phys. Rev. Lett.*, 69:1006–1009, Aug 1992. doi: 10.1103/PhysRevLett.69.1006. URL <https://link.aps.org/doi/10.1103/PhysRevLett.69.1006>.
- [25] Sarah Vigeland, Nicolas Yunes, and Leo Stein. Bumpy Black Holes in Alternate Theories of Gravity. *Phys. Rev. D*, 83:104027, 2011. doi: 10.1103/PhysRevD.83.104027.
- [26] Dimitry Ayzenberg and Nicolas Yunes. Slowly-Rotating Black Holes in Einstein-Dilaton-Gauss-Bonnet Gravity: Quadratic Order in Spin Solutions. *Phys. Rev. D*, 90:044066, 2014. doi: 10.1103/PhysRevD.90.044066. [Erratum: *Phys.Rev.D* 91, 069905 (2015)].

- [27] Nicolas Yunes and Frans Pretorius. Dynamical Chern-Simons Modified Gravity. I. Spinning Black Holes in the Slow-Rotation Approximation. *Phys. Rev. D*, 79: 084043, 2009. doi: 10.1103/PhysRevD.79.084043.
- [28] James M Bardeen. Non-singular general-relativistic gravitational collapse. In *Proc. Int. Conf. GR5, Tbilisi*, volume 174, page 174, 1968.
- [29] Rahul Kumar, Sushant G. Ghosh, and Anzhong Wang. Gravitational deflection of light and shadow cast by rotating Kalb-Ramond black holes. *Phys. Rev. D*, 101(10):104001, 2020. doi: 10.1103/PhysRevD.101.104001.

Appendix A

Example Theories

This appendix lists the six example beyond-GR theories considered in this thesis, whose black hole metrics can be mapped to the CY metric. For each example theory, we list some references, key parameters controlling their deviation from Kerr, mapping functions for the original and refined (rescaled and small deviation) CY metrics, and the event horizon location found by solving $1/g_{rr} = 0$. For the mapping functions for the CY metric with small deviation approximation, we only present the expressions for Approach 3 ($n = 0$) since the expressions for other n can be easily obtained by scaling appropriately with Δ^n .

A.1 Braneworld

- metric given in [21]
- parameters: tidal charge β

- original CY mapping:

$$\mathcal{A}_0(r) \rightarrow \frac{\Delta}{\Delta + \beta} \quad (\text{A.1})$$

$$\mathcal{A}_1(r) \rightarrow \frac{\Delta}{\Delta + \beta} \quad (\text{A.2})$$

$$\mathcal{A}_2(r) \rightarrow \frac{\Delta}{\Delta + \beta} \quad (\text{A.3})$$

$$\mathcal{A}_5(r) \rightarrow \frac{\Delta + \beta}{\Delta} \quad (\text{A.4})$$

$$f(r) \rightarrow 0 \quad (\text{A.5})$$

- rescaled CY mapping:

$$\bar{\mathcal{A}}_0(r) \rightarrow 1 \quad (\text{A.6})$$

$$\bar{\mathcal{A}}_1(r) \rightarrow 1 \quad (\text{A.7})$$

$$\bar{\mathcal{A}}_2(r) \rightarrow 1 \quad (\text{A.8})$$

$$\bar{\mathcal{A}}_5(r) \rightarrow \Delta + \beta \quad (\text{A.9})$$

- small deviation CY mapping with $n = 0$, exact in r:

$$\delta\mathcal{A}_0 \rightarrow \frac{\beta}{\Delta} \quad (\text{A.10})$$

$$\delta\mathcal{A}_1 \rightarrow \frac{\beta}{\Delta} \quad (\text{A.11})$$

$$\delta\mathcal{A}_2 \rightarrow \frac{\beta}{\Delta} \quad (\text{A.12})$$

$$\delta\mathcal{A}_5 \rightarrow -\frac{\beta}{\Delta} \quad (\text{A.13})$$

- event horizon location:

$$r_{EH} = M + \sqrt{M^2 - a^2 - \beta^2} \quad (\text{A.14})$$

A.2 Kerr-Sen

- metric given in [24]
- parameters: b related to magnetic dipole moment
- original CY mapping:

$$\mathcal{A}_0(r) \rightarrow \frac{(a^2 + r^2 + 2br)\Delta}{(a^2 + r^2)(\Delta + 2br)} \quad (\text{A.15})$$

$$\mathcal{A}_1(r) \rightarrow \frac{(a^2 + r^2 + 2br)^2 \Delta}{(a^2 + r^2)^2 (\Delta + 2br)} \quad (\text{A.16})$$

$$\mathcal{A}_2(r) \rightarrow \frac{\Delta}{\Delta + 2br} \quad (\text{A.17})$$

$$\mathcal{A}_5(r) \rightarrow \frac{\Delta + 2br}{\Delta} \quad (\text{A.18})$$

$$f(r) \rightarrow 2br \quad (\text{A.19})$$

- rescaled CY mapping:

$$\bar{\mathcal{A}}_0(r) \rightarrow \frac{a^2 + r^2 + 2br}{a^2 + r^2} \quad (\text{A.20})$$

$$\bar{\mathcal{A}}_1(r) \rightarrow \frac{(a^2 + r^2 + 2br)^2}{(a^2 + r^2)^2} \quad (\text{A.21})$$

$$\bar{\mathcal{A}}_2(r) \rightarrow 1 \quad (\text{A.22})$$

$$\bar{\mathcal{A}}_5(r) \rightarrow \Delta + 2br \quad (\text{A.23})$$

- small deviation CY mapping with $n = 0$, exact in r :

$$\delta\mathcal{A}_0 \rightarrow \frac{-4bMr^2}{(a^2 + r^2)\Delta} \quad (\text{A.24})$$

$$\delta\mathcal{A}_1 \rightarrow \frac{2br(\Delta - 2Mr)}{(a^2 + r^2)(\Delta - 2Mr)} \quad (\text{A.25})$$

$$\delta\mathcal{A}_2 \rightarrow \frac{-2br}{\Delta} \quad (\text{A.26})$$

$$\delta\mathcal{A}_5 \rightarrow \frac{2br}{\Delta} \quad (\text{A.27})$$

$$\delta f(r) \rightarrow 2br \quad (\text{A.28})$$

- event horizon location:

$$r_{EH} = M - b + \sqrt{(M - b)^2 - a^2} \quad (\text{A.29})$$

A.3 EdGB

- metric given in [26]
- parameters: coupling constant ζ
- original CY mapping:

$$\mathcal{A}_0(r) \rightarrow \frac{4M^5r^2\zeta + 2M^4r^3\zeta + 4M^3r^4\zeta - 96M^7\zeta + 30Mr^6 - 15r^7}{30Mr^6 - 15r^7 + 400M^7\zeta - 96M^6r\zeta - 66M^5r^2\zeta - 130M^4r^3\zeta - 5M^3r^4\zeta} \quad (\text{A.30})$$

$$\mathcal{A}_1(r) \rightarrow \frac{15(2M - r)r^6}{30Mr^6 - 15r^7 + 400M^7\zeta - 96M^6r\zeta - 66M^5r^2\zeta - 130M^4r^3\zeta - 5M^3r^4\zeta} \quad (\text{A.31})$$

$$\mathcal{A}_5(r) \rightarrow -15r^6(-2M + r)$$

$$\begin{aligned} & \times (30Mr^6 - 15r^7 - 1840M^7\zeta + 48M^6r\zeta + 30M^5r^2\zeta + 260M^4r^3\zeta \\ & + 15M^3r^4\zeta + 15M^2r^5\zeta)^{-1} \end{aligned} \quad (\text{A.32})$$

$$f(r) \rightarrow 0 \quad (\text{A.33})$$

Note there is no mapping function $\mathcal{A}_2(r)$. This is because the EdGB metric that can be mapped to the CY metric is only valid to first order in spin and $\mathcal{A}_2(r)$ appears in terms with higher order in spin in the original CY metric.

- rescaled CY mapping:

We do not show the rescaled CY mappings for EdGB as the expressions are quite long. Note there is no mapping function $\bar{\mathcal{A}}_2(r)$. This is because EdGB is valid to first order in spin and $\bar{\mathcal{A}}_2(r)$ appears in the original CY metric only in terms with higher orders in spin.

- small deviation CY mapping with $n = 0$:

$$\delta\mathcal{A}_0 \rightarrow \frac{M^3(-496M^4 + 96M^3r + 70M^2r^2 + 132Mr^3 + 9r^4)\zeta}{15(2M - r)r^6} \quad (\text{A.34})$$

$$\delta\mathcal{A}_0 \rightarrow -\frac{M^3(400M^4 - 96M^3r - 66M^2r^2 - 130Mr^3 - 5r^4)\zeta}{15(2M - r)r^6} \quad (\text{A.35})$$

$$\delta\mathcal{A}_5 \rightarrow \frac{M^2(1840M^5 - 48M^4r - 30M^3r^2 - 260M^2r^3 - 15Mr^4 - 15r^5)\zeta}{15(2M - r)r^6} \quad (\text{A.36})$$

- event horizon location:

$$r_{EH} = 2M \quad (\text{A.37})$$

A.4 dCS

- metric given in [27]
- parameters: coupling constant ζ
- original CY mapping:

$$\mathcal{A}_0(r) \rightarrow 1 - \frac{27M^6\zeta}{16r^6} - \frac{15M^5\zeta}{14r^5} - \frac{5M^4\zeta}{8r^4} \quad (\text{A.38})$$

$$\mathcal{A}_1(r) \rightarrow 1 \quad (\text{A.39})$$

$$\mathcal{A}_5(r) \rightarrow 1 \quad (\text{A.40})$$

$$f(r) \rightarrow 0 \quad (\text{A.41})$$

There is no mapping function $\mathcal{A}_2(r)$ for the same reason as in EdGB.

- rescaled CY mapping:

$$\bar{\mathcal{A}}_0(r) \rightarrow 1 - \frac{27M^6\zeta}{16r^6} - \frac{15M^5\zeta}{14r^5} - \frac{5M^4\zeta}{8r^4} \quad (\text{A.42})$$

$$\bar{\mathcal{A}}_1(r) \rightarrow 1 \quad (\text{A.43})$$

$$\bar{\mathcal{A}}_5(r) \rightarrow \Delta \quad (\text{A.44})$$

Note there is no mapping function $\bar{\mathcal{A}}_2(r)$. This is because dCS is valid to first order in spin and $\bar{\mathcal{A}}_2(r)$ appears in terms with higher order spin in the refined CY metric.

- small deviation CY mapping with $n = 0$, exact in r :

$$\delta\mathcal{A}_0 \rightarrow -\frac{M^4(189M^2 + 120Mr + 70r^2)\zeta}{112r^6} \quad (\text{A.45})$$

$$\delta\mathcal{A}_1 \rightarrow 0 \quad (\text{A.46})$$

$$\delta\mathcal{A}_5 \rightarrow 0 \quad (\text{A.47})$$

- event horizon location:

$$r_{EH} = 2M \quad (\text{A.48})$$

A.5 Bardeen

- metric given in [28]
- parameters: g controls regularity of the black hole
- original CY mapping:

$$\mathcal{A}_0(r) \rightarrow \frac{\Delta(g^2 + r^2)^{3/2}}{(a^2 + r^2)(g^2 + r^2)^{3/2} - 2Mr^4} \quad (\text{A.49})$$

$$\mathcal{A}_1(r) \rightarrow \frac{\Delta(g^2 + r^2)^{3/2}}{(a^2 + r^2)(g^2 + r^2)^{3/2} - 2Mr^4} \quad (\text{A.50})$$

$$\mathcal{A}_2(r) \rightarrow \frac{\Delta(g^2 + r^2)^{3/2}}{(a^2 + r^2)(g^2 + r^2)^{3/2} - 2Mr^4} \quad (\text{A.51})$$

$$\mathcal{A}_5(r) \rightarrow \frac{(a^2 + r^2)(g^2 + r^2)^{3/2} - 2Mr^4}{\Delta(g^2 + r^2)^{3/2}} \quad (\text{A.52})$$

$$f(r) \rightarrow 0 \quad (\text{A.53})$$

- rescaled CY mapping:

$$\bar{\mathcal{A}}_0(r) \rightarrow 1 \quad (\text{A.54})$$

$$\bar{\mathcal{A}}_1(r) \rightarrow 1 \quad (\text{A.55})$$

$$\bar{\mathcal{A}}_2(r) \rightarrow 1 \quad (\text{A.56})$$

$$\bar{\mathcal{A}}_5(r) \rightarrow a^2 + r^2 - \frac{2Mr^4}{(g^2 + r^2)^{3/2}} \quad (\text{A.57})$$

- small deviation CY mapping with $n = 0$, exact in r :

$$\delta\mathcal{A}_0 \rightarrow -\frac{3g^2M}{r\Delta} \quad (\text{A.58})$$

$$\delta\mathcal{A}_1 \rightarrow -\frac{3g^2M}{r\Delta} \quad (\text{A.59})$$

$$\delta\mathcal{A}_2 \rightarrow -\frac{3g^2M}{r\Delta} \quad (\text{A.60})$$

$$\delta\mathcal{A}_0 \rightarrow \frac{3g^2M}{r\Delta} \quad (\text{A.61})$$

- event horizon location: We were not able to find a closed-form expression for the horizon location for the Bardeen black hole. Instead, we assume $g \ll M < r$ and find r_{EH} perturbatively:

$$r_{EH} = r_0 - \frac{3M^3r_0}{4M^2r_0 - 2a^2(M + r_0)} \frac{g^2}{M^2} + \mathcal{O}\left(\frac{g^4}{M^4}\right), \quad (\text{A.62})$$

where $r_0 = M + \sqrt{M^2 - a^2}$ is the Kerr horizon location.

A.6 Kalb-Ramond

- metric given in [29]

- parameters: Kalb-Ramond parameter s and Lorentz-violating parameter Γ . We choose $s = 2$ in this work.

- original CY mapping:

$$\mathcal{A}_0(r) \rightarrow \frac{\Delta r^{\frac{2}{s}}}{r^{2+\frac{2}{s}} + a^2 r^{\frac{2}{s}} - 2Mr^{\frac{2+s}{s}} + r^2\Gamma} \quad (\text{A.63})$$

$$\mathcal{A}_1(r) \rightarrow \frac{\Delta r^{\frac{2}{s}}}{r^{2+\frac{2}{s}} + a^2 r^{\frac{2}{s}} - 2Mr^{\frac{2+s}{s}} + r^2\Gamma} \quad (\text{A.64})$$

$$\mathcal{A}_2(r) \rightarrow \frac{\Delta r^{\frac{2}{s}}}{r^{2+\frac{2}{s}} + a^2 r^{\frac{2}{s}} - 2Mr^{\frac{2+s}{s}} + r^2\Gamma} \quad (\text{A.65})$$

$$\mathcal{A}_5(r) \rightarrow \frac{r^{2+\frac{2}{s}} + a^2 r^{\frac{2}{s}} - 2Mr^{\frac{2+s}{s}} + r^2\Gamma}{\Delta r^{\frac{2}{s}}} \quad (\text{A.66})$$

$$f(r) \rightarrow 0 \quad (\text{A.67})$$

- rescaled CY mapping:

$$\bar{\mathcal{A}}_0(r) \rightarrow 1 \quad (\text{A.68})$$

$$\bar{\mathcal{A}}_1(r) \rightarrow 1 \quad (\text{A.69})$$

$$\bar{\mathcal{A}}_2(r) \rightarrow 1 \quad (\text{A.70})$$

$$\bar{\mathcal{A}}_5(r) \rightarrow \Delta + r^{\frac{2}{s}(s-1)} \quad (\text{A.71})$$

- small deviation CY mapping with $n = 0$, exact in r :

$$\delta\mathcal{A}_0 \rightarrow -\frac{r^{2-\frac{2}{s}}\Gamma}{\Delta} \quad (\text{A.72})$$

$$\delta\mathcal{A}_1 \rightarrow -\frac{r^{2-\frac{2}{s}}\Gamma}{\Delta} \quad (\text{A.73})$$

$$\delta\mathcal{A}_2 \rightarrow -\frac{r^{2-\frac{2}{s}}\Gamma}{\Delta} \quad (\text{A.74})$$

$$\delta\mathcal{A}_5 \rightarrow \frac{r^{2-\frac{2}{s}}\Gamma}{\Delta} \quad (\text{A.75})$$

$$(\text{A.76})$$

- event horizon location: This horizon location was calculated for Kalb-Ramond parameter $s = 2$.

$$r_{EH} = \frac{2M - \Gamma + \sqrt{(\Gamma - 2M)^2 - 4M^2}}{2} \quad (\text{A.77})$$

Appendix B

RMSE with varied θ and a

In our analysis, we began calculating which values of θ and a would yield the maximum RMSE values for the small deviation approximation method. θ values were varied between 0 and π while a values were varied between 0 and 1. Both parameters were varied simultaneously.

Here we show those values for the Braneworld example. Approaches 1, 2, and 3 with the exact expression in r for the mapping functions in the small deviation approximation were all able to recover Braneworld exactly, as well as Approach 1 with the mapping functions expanded in r . We therefore show only the maximized RMSE values for Approaches 2 ($n = 0$), and 3 ($n = 1$). The RMSE values for all tt , rr , and $t\phi$ components for this Braneworld example are maximized when $\theta = 2.61304$ and $a = 0.918921$, meaning CY performs the worst when θ and a take these values. The results are summarized in Table [B.1](#).

A similar analysis can be done with the five other example metrics given in Appendix [A](#) to investigate which values of θ and a will maximize their RMSEs.

Approach	Component	UIL [r_{EH}]	RMSE	θ	a
2 ($n = 0$)	tt	2	1.55×10^{-1}	2.61304	0.918921
		100	2.55×10^{-3}	2.61304	0.918921
	rr	2	1.27×10^{-1}	2.61304	0.918921
		100	2.55×10^{-3}	2.61304	0.918921
	$\phi\phi$	2	3.37×10^{-3}	1.79845	0.896642
		100	2.52×10^{-7}	1.79845	0.896642
	$t\phi$	2	2.63×10^{-2}	2.61304	0.918921
		100	1.68×10^{-2}	2.61304	0.918921
3 ($n = 1$)	tt	2	1.65×10^{-1}	2.61304	0.918921
		100	2.76×10^{-3}	2.61304	0.918921
	rr	2	1.36×10^{-1}	2.61304	0.918921
		100	2.76×10^{-3}	2.61304	0.918921
	$\phi\phi$	2	5.65×10^{-3}	2.02787	0.941569
		100	2.82×10^{-7}	1.79845	0.896642
	$t\phi$	2	2.81×10^{-2}	2.61304	0.918921
		100	1.82×10^{-2}	2.61304	0.918921

Table B.1: RMSE values maximized by varying θ and a for the Braneworld black hole with Approaches 2 ($n = 0$) and 3 ($n = 1$) with the mapping functions expanded in r . The other parameter values were chosen as $M = 1$ and $\beta = 0.1$.

Appendix C

Konoplya-Rezzolla-Zhidenko

Metric

Konoplya, Rezzolla, and Zhidenko [19] present another generic, theory-agnostic beyond-Kerr metric. Their metric takes the form:

$$ds^2 = -\frac{N^2(r, \theta) - W^2(r, \theta) \sin^2 \theta}{K^2(r, \theta)} dt^2 - 2W(r, \theta) r \sin^2 \theta dt d\phi + K^2(r, \theta) r^2 \sin^2 \theta d\phi^2 + \Sigma(r, \theta) \left(\frac{B^2(r, \theta)}{N^2(r, \theta)} dr^2 + r^2 d\theta^2 \right). \quad (\text{C.1})$$

Let us call this metric the KRZ metric. It contains five functions of the radial coordinate r and the polar coordinate θ , $N(r, \theta)$, $W(r, \theta)$, $K(r, \theta)$, $B(r, \theta)$, and $\Sigma(r, \theta)$, that encompass deviations from Kerr. They utilize a double expansion to find their beyond-Kerr coefficients – the first expansion is about $r = \infty$ followed by a second continued fraction expansion near the horizon.

We were interested to investigate if their metric formulation yields similar patholo-

gies to the original CY metric parameterization seen with the Braneworld example. They report mapping functions and coefficients in [19] for two beyond-GR metrics, Kerr-Sen and EdGB. Before trying to map their metric to Braneworld, we worked through their procedure to see if we could reproduce the same mapping functions and coefficients for KRZ mapped to Kerr-Sen. The mapping functions for Kerr-Sen are given in Equation (56) in [19] and the expansion coefficients are given in Equations (58) through (60).

We were able to reproduce all mapping functions and coefficients, except the coefficient w_{01} . We found w_{01} given in equation (60f) of [19] to be off by a minus sign. We saw no divergences or pathological behavior in the KRZ reconstructions of the Kerr-Sen metric.

Following this, we began a similar analysis to determine the mapping functions and coefficients for Braneworld. As of the time of writing this thesis, this is still a work in progress. Thus far, we have found three coefficients for Braneworld:

$$\epsilon_0 = \frac{2M}{r_{EH}} - 1 \quad (\text{C.2})$$

$$a_{00} = \frac{\beta}{r_{EH}^2} \quad (\text{C.3})$$

$$k_{00} = \frac{a^2}{r_{EH}^2} \quad (\text{C.4})$$

where r_{EH} is the event horizon location for Braneworld.

We have also begun to implement a double expansion on the small deviation approximation with ($n = 1$) of the CY metric mapped to Kerr-Sen. That is, we expand the mapping functions both at infinity and at the event horizon. In this

analysis, we follow the convention of using compactified coordinates $x \equiv 1 - \frac{r_{EH}}{r}$ in the same way Konoplya, Rezzolla, and Zhidenko do in their analysis. We expand the $\delta\mathcal{A}_i$ functions about $x = 1$, or $r = \infty$, and keep to third order, for example. We then expand the coefficient of the third order term about $x = 0$, or $r = r_{EH}$. We can then read off coefficients from these expansions, and plug them back in to the CY metric with the small deviation approximation. Figure C.1 shows the preliminary result of applying the double expansion to the tt component of CY mapped to Kerr-Sen with the $n = 1$ small deviation approximation. We see CY with the double expansion agrees with the true Kerr-Sen metric at spatial infinity, $x = 1$, but does not agree at the horizon, $x = 0$. The reason for this disagreement at the horizon will need further investigation.

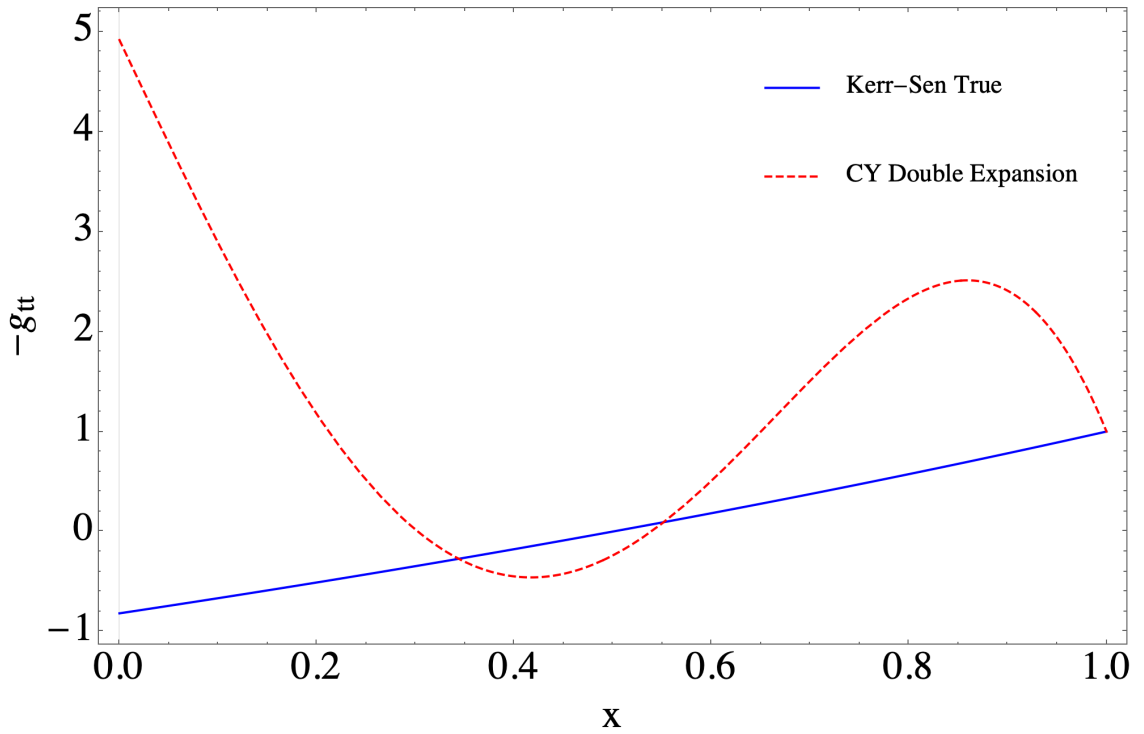


Figure C.1: tt component of the $n = 1$ small deviation approximation CY metric mapped to Kerr-Sen with double expansion. In this analysis, we choose parameter values $\theta = \frac{\pi}{2}$, $a = 0.9$, $M = 1$, and $b = 0.1$.